The Pennsylvania State University

The Graduate School

College of Earth and Mineral Sciences

CARBON AND HYDROGEN ISOTOPIC COMPOSITION OF METHANE OVER THE LAST 1000 YEARS

A Thesis in

Geosciences

by

John A. Mischler

Submitted in Partial Fulfillment
of the Requirements
for the Degree of

Master of Science

May 2009

The thesis of John A. Mischler was reviewed and approved* by the following:

Richard B. Alley
Evan Pugh Professor of Geosciences
Thesis Co-Advisor

Todd A. Sowers
Senior Research Associate in Geosciences
Thesis Co-Advisor

Michael E. Mann
Professor of Geosciences and Meteorology

Katherine H. Freeman
Professor of Geosciences
Associate Head for Graduate Programs and Research in Geosciences

* Signatures are on file in the Graduate School

Abstract

New measurements of the carbon and hydrogen isotopic ratios of methane (δ^{13}C of CH_4 and δD of CH_4) over the last millennium are presented from the WAIS Divide, Antarctica ice core (WDC05A), showing significant changes that likely were influenced by humans even before the industrial revolution. The δ^{13}C of CH_4 data corroborate the record from Law Dome, Antarctica with high fidelity. The new δD of CH_4 data set covaries with the $\delta^{13}CH_4$ record. Both δ^{13}C of CH_4 and δD of CH_4 were relatively stable and close to the present-day values from 1000 to ∼1500 CE. Both isotopic ratios decreased to minima around 1700 CE, remained low until the late 18th century, and then rose exponentially to present-day values. Our new δD of CH_4 data provide an additional independent constraint for evaluating possible CH_4 source histories. We searched a broad range of source scenarios using a simple box model to identify histories consistent with the constraints of the CH_4 concentration and isotope data from 990-1730 CE. Results typically show a decrease over time in the biomass-burning source (found in 85% of acceptable scenarios) and an increase in the agricultural source (found in 77% of acceptable scenarios), indicating preindustrial human influence on atmospheric methane.

Table of Contents

List of Tables

List of Figures

Acknowledgments

Thanks to Todd who has spent a large amount of time teaching me how to generate good data sets. He has helped me to persevere through set backs and difficulties in order to obtain the data presented here. His help forming this thesis has been very valuable.

Thanks to Richard who has spent many many hours helping me to refine this thesis and developing the story told in this work. He has taught me how to effectively report my findings to an audience and has been instrumental in putting together the modeling section.

Thanks to Mike Mann who was been a valuable source for understanding variations in the climate system over the last millennium.

A huge thanks goes to my wife Ruth Mischler. She has seen me through all the toil associated with this thesis and has supported me the whole way. Here selfless loyalty and gracious example has shown me what it is to be loved.

Thanks to Isaac Gerg who has spent hours helping me write MATLAB code and was instrumental in developing my model approach.

Thanks to my office mates Brian Levay who has always been around to answer my questions, and Roman Tonkonojenkov who helped me make my model run more efficiently.

Thanks to Denny Walizer who spent tireless hours not only keeping all the machines going but also helping my fix what I messed up.

Thanks to God who makes all things possible.

1 Introduction

Methane plays an important role in both atmospheric chemistry and the radiative balance of the Earth [Reeburgh, 2004]. Ice cores provide high-resolution archives of the concentrations and isotopic ratios (δD and δ^{13}C) of methane [Fischer et al., 2008; Meure et al., 2006; Sowers, 2006; Ferretti et al., 2005; Sowers et al., 2005; Etheridge et al., 1998]. CH_4 concentration measurements can be used to constrain CH_4 flux estimates (involving sources and sinks of CH_4) over time while CH_4 isotope values provide additional information that is useful for resolving the relative importance of individual sources and sinks. Natural sources of CH_4 include wetlands, wildfires, termites, and ocean sediments, while rice paddies, ruminants, landfills, natural gas extraction, and biomass burning are the major anthropogenic sources (extensive review by Reeburgh [2004]). The isotopic compositions of different sources have been measured over various temporal and spatial scales to estimate characteristic values of δD and δ^{13}C for each source (Table 5). The δ^{13}C and δD measurements of CH_4 ($\delta^{13}CH_4$ and $\delta D(CH_4)$ respectively) clearly distinguish isotopically enriched sources (biomass burning and natural gas venting) from depleted sources (wetlands and rice paddies).

Because there are more distinct methane source types than isotopic tracers, and more spatially distributed sources than can be resolved by the geographically restricted suite of ice cores (only the ice cores of Antarctica and Greenland are known to provide reliable methane records), a unique inversion for the history of methane sources is not possible. However, the full suite of isotopic tracers and bipolar ice core data provide important tests of hypotheses for methane source histories, allowing elimination of large classes of scenarios.

1.1 Previous work

Ferretti et al. [2005] generated the first high-resolution $\delta^{13}CH_4$ record covering the last two millennia. Their record showed $\delta^{13}CH_4$ values that are very similar to present-day values between 0 and 1500 CE. After 1500 CE, their record exhibited an unexpected 2‰ decrease while the CH_4 concentration varied by less than 40 ppb (∼2%). A broad $\delta^{13}CH_4$ minimum (-49‰) persisted for about one century before increasing to present-day values (-47‰). This last $\delta^{13}CH_4$ change occurred during a period when the CH_4 loading of the atmosphere increased by over 100%, and is largely the result of additional anthropogenic sources that have enriched $\delta^{13}CH_4$ values. Ferretti et al. [2005] explained their results in terms of high baseline emissions of enriched CH_4 from biomass burning prior to 1500 CE. The decreasing $\delta^{13}CH_4$ values between 1500 and 1700 CE were ascribed to a decrease in biomass burning associated with a decline in world population centered in Central and South America following European contact.

An alternate interpretation of the $\delta^{13}CH_4$ record was presented by Houweling et al. [2008], who attributed the heavy $\delta^{13}C$ values prior to 1500 CE to elevated emissions of aerobic methane from plants (as discussed in Keppler et al. [2006]). Houweling et al. [2008] ascribed the drop in $\delta^{13}CH_4$ between 1500 and 1700 CE to the effects of an increase in the agricultural source (rice farming and animal husbandry) scaled to world population, in tandem with reduced plant growth and wetland emissions caused by the cooling of the Little Ice Age (LIA). Houweling et al. [2008] noted that this hypothesis pressed the limits of both the maximum published temperature change for the LIA [Moberg et al., 2005] as well as the relationship between temperature and methane emissions. Also, it should be noted that the significance of the aerobic plant source has recently been called into question [Dueck et al., 2007].

In this contribution we provide new records of $\delta^{13}CH_4$ and $\delta D(CH_4)$ covering the last 1000 years from the WAIS Divide ice core WDC05A. While we present data covering the entire 1000 year period, our discussion will only focus on the

period between 990 and 1730 CE. We limit our discussion to this 740 year period in order to refine our understanding of the decoupling between the relatively constant atmospheric loading record and the unexpectedly large change in $\delta^{13}CH_4$. Model results using our new isotope records along with existing concentration records suggest changes in anthropogenic sources (that are proportional to global population) likely had a large impact on the atmospheric CH_4 budget during this period.

1.2 Chronology Development

The WDC05A core (79° 27.7' S 112° 7.51' W, 1,759masl) was drilled to 298.06m during December of 2005. The drill site was located 1.3km from the main WAIS Divide drill site, with a primary objective of reconstructing high-resolution atmospheric records covering the last 1,000 years. The upper 70m of the core was processed for continuous ion chemistry [McConnell et al., 2002], providing the most accurate means of constructing the ice age vs. depth model, with an absolute uncertainty of ± 1yr. In addition, continuous electrical conductivity and dielectric property (ECM/DEP) data were used to count annual layers over the entire core. The ECM/DEP records were independently counted by two individuals. The resulting age models agreed with one another within ± 5%. The final ice age vs. depth model was constructed using the major ion data for the upper 70m and the ECM/DEP counts from 70m to 298m.

The age of the occluded gases is younger than the surrounding ice because air diffuses down through the firn more rapidly than snow is buried to the depth of bubble trapping in the firn/ice transition region (65-75 meters below surface (mbs)). To estimate the ice age - gas age difference (Δage), a 1-D model of gas transport in the firn was developed for the site, following Battle et al. [1996] and Trudinger et al. [1997]. The transport model was used to estimate a mean gas age of 9.9 years at the top of the lock-in zone (65.5mbs). The ice age at this level was 215 years at the time

of coring, making Δage equal to 205.1 years. The gas age vs depth model for the WDC05A core was established by subtracting 205.1 years from the ice age at every dated depth below 65.5mbs. We estimate the uncertainty associated with the gas age assignment as $\pm$ 5%, but note that comparison of the detailed CH_4 record from WDC05A with the Law Dome CH_4 record from Meure et al. [2006] suggests our gas age model is probably good to within a decade relative to the Law Dome chronology (Mitchell et al., manuscript in prep.).

2 Analytical Methods

The "wet" extraction procedures used in this study for liberating relict air from ice samples followed by mass spectrometric determination of the δD(CH_4) and $\delta^{13}CH_4$ were similar to those described by Sowers [2006] and Sowers et al. [2005] respectively. Ice samples between 1-1.6 kg for δD (0.4-0.7 kg for δ^{13}C) were cut from larger core sections in order to obtain sufficient amounts of trapped CH_4 for δD and $\delta^{13}CH_4$ analysis. Between the base of the firn-ice transition (75mbs) and the bottom of the core (298.06mbs) a total of 58 samples were analyzed for $\delta^{13}CH_4$ and 40 samples for δD(CH_4). This sampling strategy yielded records that have a resolution of 20 years for both the δD and $\delta^{13}CH_4$ records from the 15^{th} century to around the 1970s (although there is a notable gap in the $\delta^{13}CH_4$ data from the late 16^{th} century through the late 17^{th} century), with lower resolution sampling for both records stretching back to around the 1160s CE (and into the first millennium CE for $\delta^{13}CH_4$). The δD(CH_4) record contains small gaps in the data set centered around the late 1790s and the 1930s, while minor gaps are apparent in the $\delta^{13}CH_4$ data in the late 18^{th} century and late 19^{th} century. A uniformly sampled data set was not achieved because: 1)some areas did not have sufficient good-quality ice; and/or 2), problems were encountered during the extraction/analytical procedure.

2.1 Sample processing and analysis

The outer ∼5mm of each core section was shaved away using a band saw to expose fresh ice core. Each shaved ice sample was sealed into a stainless steel (SS) cylinder using a copper gasket, and evacuated for 1 hour to remove the ambient air from the sample cylinder and sublimate a thin film of ice from the sample. The evacuated cylinder was then isolated and placed within a $\sim$ 40 °C warm water bath (45 min

for δD, 30 min for δ^{13}C) to completely melt the ice sample and release the trapped relict air into the headspace of the cylinder above the meltwater. The cylinder was then placed into a large SS Dewar where the meltwater was refrozen using liquid nitrogen. After the meltwater was completely frozen (45 min for δD, 30 min for δ^{13}C), the sample cylinder was connected to the evacuated extraction line. The cylinder headspace was flushed with ultra-high purity (UHP) He (40 cc/min) until the relict air was quantitatively removed from the cylinder (one hour for δD, 45 min for δ^{13}C). It was determined that more than ∼90% of the relict air originally trapped in the ice was liberated and flushed from the cylinder into the extraction system. The sample air was moved from the cylinder, through a water trap ($-110\,^{\circ}$C) and a methane trap (HaySep D at $-130\,^{\circ}$C). The CH_4 in the relict air adsorbed onto the HaySep D material in the methane trap. The methane trap was then isolated and removed from the extraction system and attached to a PreCon peripheral device for CH_4 isotopic analysis following Sowers et al. [2005] and Sowers [2006].

2.2 Method verification, corrections, and uncertainties

An independent house standard (CA 04826) ($\delta^{13}C_{assigned}$ = -47.13±0.01‰, $\delta D_{assigned}$ = -84.3±1.6‰) was used to establish the integrity of the extraction process at various times during the period when we extracted the ice samples (Table 1). This high-pressure air cylinder was filled during a research cruise in the South Pacific [Rice et al., 2001], and assigned CH_4 isotope values based on analyses by Stan Tyler at the University of California, Irvine. Glass flasks (50-200 cc) containing the house standard CA 04826 were equilibrated and analyzed directly at the beginning of each day before sample runs. If the daily standard runs differed too much (∼0.2‰ for δ^{13}C and ∼3‰ for δD) from the mean value of the average of recent previous runs, additional standards were run until a stable isotope value for the standard was obtained.

These standard measurements (100 for δ^{13}C and 36 for δD) resulted in mean

values for the standard CA 04826 samples on our system (-46.9±0.1‰ for δ^{13}C and -86±3‰ for δD) that were offset (∼0.2‰ for δ^{13}C and ∼-2‰ for δD) from the values determined by Tyler (Table 1). Great efforts have been made to minimize the offset between the daily measurements and the assigned values. We believe the offset stems from long-term drift in the oxidation/thermal conversion furnaces, which are difficult to control on a day-to-day-basis. To account for these day-to-day furnace fluctuations, we have chosen to correct all samples run on a particular day for the difference between the measured standard value and the assigned value. The magnitude of this correction is generally less than 0.2‰ and 3‰ for δ^{13}C and δD, respectively. This correction assumes the offset is nearly constant throughout a day of measurements, which we have verified by running multiple standards during some days.

Additionally, the δD data must be corrected for what is termed the "viscous flow effect". In our D/H analytical technique, reference peaks for each run are introduced into the mass spectrometer source from the bellows as opposed to the gas bench where the sample comes in. An experiment was performed to determine the zero enrichment of this system by placing an aliquot of UHP (5.0) H_2 from a large tank feeding the Gas Bench into the bellows of the mass spectrometer and running it against the original tank via the Gas Bench. The resulting zero enrichment showed substantial offset that scaled with the pressure in the bellows (higher offset at lower bellows pressure). We surmise that the offset arises at the capillary crimp where the pure H_2 from the bellows passes into a He background in the source. The viscous flow correction is performed numerous times during a week at the pressures equivalent to our normal working standard, and must be redefined for any change in source focus or H_3 factor determination. The H_3 factor as described by Sessions et al. [2001] corrects for H_3 created in the source from the H_2 sample gas, thereby eliminating the error introduced by H_3 being mistakenly counted as HD+ by the mass spectrometer.

The extraction system was tested by expanding an aliquot of the house standard

(CA 04826) over bubble-free ice (BFI) produced in the lab, then sealed in a cylinder and processed in the same manner as the samples. The BFI was run through a freeze/thaw cycle, and the resulting headspace gas was flushed through the extraction system as described previously. This process was repeated 16 times for $\delta^{13}CH_4$ (mean value = -47.4±0.2‰, -0.3‰ from the assigned value) and five times for $\delta D(CH_4)$ (mean value = -85±2, -1‰ from the assigned value) (Table 1). The difference between the assigned standard value and the measured value during simulated sample runs may arise from a small amount of CH_4 remaining in the ice upon refreezing. Estimates of the isotopic composition of CH_4 in equilibrium with water suggest the $\delta^{13}CH_4$ of CH_4 in the meltwater should be 0.3‰ higher than the headspace gas [Knox et al., 1992], Based on our estimate of the extraction efficiency (95%) and the partition of CH_4 between the headspace and water in the vessel, we calculate that this effect may have raised the $\delta^{13}CH_4$ in our samples by less than 0.1‰, not enough to account for the enriched nature of the simulated transfers. The remainder of the offset between the assigned value and the simulated transfer results must be the result of very small isotope fractionation processes associated with our technique.

All uncertainties for the data points were assessed based on the uncertainties measured for the simulated trapped-gas extractions, in which the standards were processed in exactly the same way as our samples, including the mass spectrometric analyses and their corresponding corrections. We believe this is the most representative means of conveying the true analytical uncertainty, yielding ±0.2‰ and ±3‰ for $\delta^{13}CH_4$ and $\delta D(CH_4)$, respectively.

Both the $\delta D(CH_4)$ and $\delta^{13}CH_4$ data sets were corrected for gravitational effects (-0.31‰) according to Sowers et al. [1989]. Gravitational fractionation in the firn is mass-dependent, such that the heavier isotopologues of CH_4 are preferentially concentrated at the base of the firn. The $\delta^{15}N$ of N_2 is constant over millions of years and also influenced by gravitational fractionation [Sowers et al., 1989]. We use

the measured $\delta^{15}N$ of N_2 at the base of the firn (+0.31‰, J. Severinghaus personal communication) to correct all our CH_4 isotope data for gravitational fractionation.

Both the $\delta D(CH_4)$ and $\delta^{13}CH_4$ data sets were also corrected for diffusional effects that arise from atmospheric concentration changes. As the concentration of an atmospheric constituent varies, the surface values are propagated down into the firn by diffusion. Because the diffusivity of a $^{13}CH_4$ molecule is 1.8% lower than for the $^{12}CH_4$ species [Trudinger et al., 1997], increasing atmospheric CH_4 produces a drop in the firn air $\delta^{13}CH_4$ relative to the overlying atmospheric value. To correct our measured values for this effect, we utilized the 1-D firn-air transport model of Battle et al. [1996] and the Law Dome CH_4 record to estimate the magnitude of the diffusion correction. The correction is largest during periods when CH_4 increases most rapidly. The largest corrections (∼1.5‰) need to be applied to the data from just below the firn/ice transition region (75-85m). We generated data for the $\delta^{13}CH_4$ during 2007 and 2008. However, due to problems encountered during the extraction procedure, only the $\delta^{13}CH_4$ measurements from 2008 are included in this study. For a detailed discussion regarding the 2007 data omitted from this study, please refer to Appendix C and Table 3. All data used in this study are tabulated in Table 2 and Table 4.

3 Analytical Results

The δD and $\delta^{13}CH_4$ trends over the last 1000 years are shown in Figure 1 along with the CH_4 concentration curve generated by Meure et al. [2006]. The $\delta^{13}CH_4$ data generated by Ferretti et al. [2005] are also displayed for comparison. There is remarkable agreement between the two $\delta^{13}CH_4$ data sets, considering they were generated from different cores with different timescales and in separate labs. This indicates that these data sets are reliable and record the past levels of $\delta^{13}CH_4$ with high fidelity. We present the first $\delta D(CH_4)$ record for this period, and note that the shape of this record is very similar to the $\delta^{13}CH_4$ record. As shown in Figure 1 both the δD and $\delta^{13}CH_4$ started to decrease at $\sim$1460 CE, which is also when CH_4 began an abrupt $\sim$30 ppb rise. Both δD and $\delta^{13}CH_4$ continued to decrease as CH_4 reversed its trend and suddenly decreased by $\sim$20 ppb starting in the 1580s CE. CH_4 remained low while δD and $\delta^{13}CH_4$ reached their lowest values until all three increased from the late 18^{th} century onward. As mentioned previously, the focus of the current contribution is the 740 year period that ends in the middle of the 18^{th} century. We have also measured ice core and firn air samples that extend these records to the present day. These data are included in Figure 1. Our $\delta^{13}CH_4$ data are in good agreement with Ferretti et al. [2005]. The $\delta D(CH_4)$ data show a trend similar to that of $\delta^{13}CH_4$ which one expects given that most industrial CH_4 sources are enriched in all heavy isotopes. We have chosen to present this data to illustrate the abrupt isotope changes that have occurred during the last century. However, as the focus of the present contribution only extends to the 18^{th} century, we do not discuss the significance of the latest isotope results in terms of specific industrial sources as this discussion is beyond the scope of our present discussion.

4 Modeling Methods

The following sections describe our use of a box model of atmospheric methane to invert for changes in source strengths consistent with the reconstructed changes in methane concentration and isotopic ratios. The atmospheric methane model used in this study has been modified from that of Tans [1997]. It consists of two perfectly-mixed boxes, corresponding to the Northern and Southern hemispheres, with an interhemispheric exchange time fixed at 1 year. The lifetime of methane (which governs the rate of methane destruction) was also held constant at 7.6 years for both hemispheres, consistent with previous work [Houweling et al., 2000b; Lassey et al., 2000; Ferretti et al., 2005]. The model allows independent methane sources in the Northern and Southern Hemispheres and a single methane sink acting on both boxes. Each model run was allowed to reach steady state for the given input parameters.

In reality there is a diverse set of methane sources and sinks, which are distributed non-uniformly across the Earth's surface. In light of the under-constrained nature of the problem, we follow previous workers by consolidating the large range of sources and sinks into a smaller number of categories. The CH_4 sources were divided into four categories: agricultural (e.g. rice farming and animal husbandry), geologic (e.g. hydrocarbon seepage and venting), natural bacterial (natural_{Bac}) (e.g. wetlands, lakes, termites, etc.), and biomass burning. Each category was assigned a unique isotopic value for both the δD and $\delta^{13}CH_4$ (Table 5), and these values were held constant while the magnitude of each category's emissions was allowed to vary from one run to the next within a range provided by the literature (references found in Table 5). The sinks were likewise consolidated into one sink term with characteristic fractionation factors for δ^{13}C and δD. The fractionation factors and relative contributions for the major sinks of methane (as described in section 4.2 and Table 6) were held constant throughout the model runs. We believe that these ranges encompass all possible combinations of emissions.

4.1 Source characterization

All source category isotopic values and emission ranges (as well as their associated references) are described in detail in Table 5. The high and low ends of the source strength ranges for each emission category were determined using the highest and lowest estimates found in the literature (references found in Table 5), in order to consider the widest range of possibilities. We believe that these ranges are somewhat broader than needed to capture actual emissions, and thus that we have successfully searched the likely combinations of emissions.

The agricultural source category contains contributions from both rice cultivation and animal husbandry. The relative contribution of each was determined using a weighted average calculated from the separate 1700 CE emission rates given in Lassey et al. [2007], which are assumed to hold for all "low-emission" time intervals before the onset of rapid global population growth in the 1730s. Rumen studies included in the averaging were restricted to those in which animals were fed a diet of primarily C3 plants; corn was not commonly used as livestock feed during the pre-industrial era [Turner et al., 2001]. The isotopic value for rice was determined by averaging the mean isotopic values from a number of rice studies conducted in both humid tropical and humid sub-tropical regions (Table 5). Numerous natural sources of bacterially-produced CH_4 are included in the natural$_{Bac}$ source category. The contribution of CH_4 from anthropogenic burning of fossil fuels before 1730 CE was taken to be negligible following Andres et al. [1999]. All isotopic values chosen for these model runs are consistent with previous studies within the uncertainty range introduced by heterogeneity of values within each source class [Levin et al., 1993; Khalil, 1993; Quay et al., 1999; Houweling et al., 2000; Lassey et al., 2000; Tyler et al., 2007].

4.2 Sink characterization

This model incorporates a single sink term with corresponding kinetic isotope effects for both the $\delta^{13}CH_4$ and $\delta D(CH_4)$ (KIE_{13C} and KIE_D respectively). In order to determine these KIEs, three key sinks of methane were identified (oxidation by tropospheric species [OH], oxidation by stratospheric species [OH, Cl and $O(^1D)$], and oxidation in soils). Another possible sink term, here called the marine boundary layer chlorine sink, has been suggested by the modeling work of Allan et al. [2007]. To date there have been no studies confirming the existence of this sink by actual Cl radical measurements and its magnitude and long-term temporal variation are not well constrained. Therefore, we follow Fischer et al. [2008] by not including this sink in our composite sink term, although we do explore how changes in the composite sink term affect the median source strengths in our sensitivity runs (discussed in section 4.5). All values used in determining the single sink term are shown in Table 6.

4.3 Modeling approach

Our approach centers on using the CH_4 concentration and isotope data in Figure 1 as target values for assessing the relative contribution of various sources with fixed characteristic isotope values. We first identified three time intervals when atmospheric CH_4 levels were reasonably constant. The first time slice (TS1) extends from 990 CE to 1460 CE when CH_4 levels averaged 684±9 ppb. TS2 extends from 1461 CE to 1575 CE when CH_4 levels were significantly higher (713±8 ppb) relative to either TS1 or TS3. Finally, TS3 extends from 1589 CE to 1730 CE when CH_4 levels dropped (689±5 ppb) before the abrupt longer term CH_4 increase to present day values began. Because the isotopic composition of atmospheric CH_4 requires a few decades to approach steady state following a perturbation [Tans, 1997], we selected isotope windows that lag the concentration windows by 20 years. Thus, the isotopic

values were taken from 1010-1480 CE corresponding to methane concentrations from 990-1460 CE, and similarly for the other windows.

For the first simulation, the model was run so that the source strengths of methane were the only parameters allowed to vary between runs, keeping all isotope values constant. The variable space defined by the ranges of source emission values in Table 5 was searched completely by the model; we call this run the primary run. A second set of runs were the initiated setting agricultural CH_4 sources to vary exponentially with population to explore the impact of this assumed scaling on calculated strengths of the other sources. Finally, a set of sensitivity runs was completed in order to evaluate whether small changes in the isotopic values of the sources (and the fractionation factors of the sinks) measurably impacted source strength medians.

A fully time-dependent inversion for source strengths would be sufficiently underconstrained that we do not attempt it. Instead, we isolate those time slices that are sufficiently long and have sufficiently stable values of methane concentration and both isotopic ratios to be considered steady-state (TS1,TS2, and TS3). For each time slice, we use the model to determine those combinations of source strengths that are consistent with the mean CH_4 concentration, $\delta^{13}CH_4$ and $\delta D(CH_4)$ in each time slice, and with the independent constraints provided by the literature and detailed in Table 5.

For each of the four sources, we stepped from the minimum to the maximum source strength (inclusive) as listed in Table 5, in increments of 1 Tg/year; we conducted model runs to steady state for every possible combination of these sources, for a total of 17,279,409 forward model runs. The partitioning of each source into northern- and southern-hemisphere boxes (partitioning shown in Table 5) was maintained the same in all runs, as were all other parameters except for the source strengths. Each model run produced a steady-state methane concentration, $\delta^{13}CH_4$ and $\delta D(CH_4)$ for each hemisphere. The output of each run was evaluated for consistency with the observed

data (CH_4 concentration, δD and $\delta^{13}CH_4$ in the southern box, which encompasses our data sources) for each of the three time slices. A result was considered to be consistent with the data if it matched all three of the constraints (concentration and both isotopic ratios) within the uncertainty in the data, which was taken as one standard deviation from the average for each constraint for each time slice. We chose to use the standard deviation instead of the standard error to constrain these ranges of allowable values in order to be more inclusive regarding possible scenarios (though we have chosen half of the conventional ± 2 standard deviations) (Figure 1, green boxes).

All runs that matched the CH_4, $\delta(CH_4)$, and $\delta^{13}CH_4$ constraints for a time period were saved. The 12,224 acceptable runs for the first time slice (TS1) (and independently, the 18,562 for the second time slice (TS2) and 57,672 for the third slice (TS3)) are displayed using a box-and-whisker plot (Figure 2, blue boxes to the left). The boxes in each figure encompass the middle 50% of the model results that best characterized the data, and the whiskers are drawn to encompass all outlying data points.

To ensure our choices for the hemispheric distribution of sources were accurate for the time period 990-1730 CE we compared the interhemispheric CH_4 gradient from our model for TS1 (inputting the primary run median source strength values of each source category from TS1) with the measured gradient [Etheridge et al., 1998]. For the median conditions, our model produces an interhemispheric gradient of 40 ppb of CH_4 for TS1 while the measured value from Etheridge et al. [1998] is 43 ± 20 ppb. Because we average CH_4 concentrations over the entire northern and southern hemispheres in our model, the model should generate an interhemispheric gradient which is smaller than the actual measured gradient. Our model gradient agrees with the actual measured gradient (within the uncertainty in the measured gradient) and therefore we have confidence in out chosen hemispheric distribution of sources.

To assess whether the strength of a particular methane source category changed significantly (with >95% confidence) within a given model run type (i.e., the primary run, the runs in which the agricultural source scaled with population, and the sensitivity runs), we followed Ott and Longnecker [2001] in calculating the two-way Wilcoxon rank sum test for the difference between the medians of the acceptable model output from TS1 to TS3. The Wilcoxon rank sum test indicates (by virtue of the very tightly constrained confidence intervals around the median values) that all changes in the median values observed within runs (from TS1 to TS3), for all model run types, are significant.

However, these tests regarding the median clearly do not capture the full distributions of the model-run outputs. In our formulation, each of the accepted source strengths in the model output for a given time interval is equally likely to be correct, so randomly choosing one value for a given source from two time intervals defines a possible history. To assess the tendency for increase, no change, or decrease within a model run type, we randomly selected 10% of the accepted model outputs for each source category for TS1 and TS3, and formed all combinations of this subset for each source category. This process was repeated for each model run type. We report our results for each source category within each run type as the percent of: 1)runs for which the particular source category increased from TS1 to TS3, 2)runs for which the particular source category did not change from TS1 to TS3 and, 3)runs for which the particular source category decreased from TS1 to TS3.

4.4 Test with the Agricultural Source Scaling with World Population

It has been proposed that agriculture, and therefore the agricultural methane source, has increased with world population over time [Pongratz et al., 2008; Ruddiman

and Thomson, 2001]. If this hypothesis is nearly correct, then it provides a way to more tightly constrain estimates of changes in other sources over time. As a means of exploring this relationship, the three median values for agricultural source emissions (one from each time slice) were taken from the primary run values as shown in Figure 2, black lines in the center of the blue boxes, and each was plotted versus the corresponding average world population from McEvedy and Jones [1978]. An exponential curve ($R^2 = 0.98$) fit these three data points better than a linear regression ($R^2 = 0.94$) and therefore was chosen to represent the relationship between the agricultural source and world population. The three agricultural source emission values were then adjusted so that they fell directly on the curve. Three separate sets of model runs, each using one of these "new" agricultural values (while all other emission ranges were varied across their full ranges, as previously stated), were then initiated. The runs for which data and model were in agreement were collected as before and plotted with the primary run on Figure 2, green boxes to the right, and the significance and sign of each indicated change was determined as done for the previous results (Table 7).

4.5 Model Sensitivity to Isotopic Variation

In all of the model runs described above, each of the four methane sources was assigned a unique $\delta^{13}CH_4$ value and $\delta D(CH_4)$ value (shown in Table 5) and each of the sinks was associated with a unique KIE (Table 6), and these were not varied. Separate sensitivity model runs were conducted to explore the effect of slight variations in these isotopic values within their uncertainties. Variations of either -1‰ $\delta^{13}CH_4$ or -5‰ $\delta D(CH_4)$ were individually applied to each source and the total sink term (+0.001 and +0.005 change to the KIE_{13C} and KIE_D respectively) in order to estimate the effect on each of the median values of the resulting source strengths. This set of ten

runs (separate shifts in carbon and in hydrogen for four source types and for the sink) was then analyzed as before, without constraining the agricultural source to follow population. The results of the sensitivity runs were then compared to the results from the primary run, using the sign test and the one-way Wilcoxon test, in order to : 1) learn whether the changes in the source medians from TS1 to TS3 that were significant in the primary runs were still significant in the sensitivity runs, 2) compare the sensitivity run data sets to the medians of the 4 source categories in the primary run in order to see if the medians of the 4 source categories differed significantly from the primary run to the sensitivity runs and, 3) determine what effect small changes in isotopic values of the source/sink terms have on the magnitudes of the source strength medians. In addition to the two-way Wilcoxon rank sum test mentioned above, we calculated the one-way Wilcoxon rank sum test [Ott and Longnecker, 2001] to examine if the data sets generated by the sensitivity runs had the same medians as corresponding medians for the primary run (with >95% confidence). None of the data sets generated in the sensitivity runs had medians that were significantly different from the corresponding medians found in the primary runs.

5 Modeling Results

5.1 Model Results for the Primary Run

As shown in the blue boxes in Figure 2, the median values of the four source strengths exhibit trends across the three time slices examined. From the first time slice (TS1) to the third time slice (TS3) there is strong evidence for an increase in the agricultural source (77% of scenarios indicate an increase from TS1 to TS3, 2% no change, 21% decrease, median change of 18 Tg/yr) (Table 7) while there is comparatively little evidence for a directional change in the geologic source (59% increase, 5% no change, 37% decrease, median change of 2 Tg/yr) or a change in the natural$_{Bac}$ source (44% increase, 1% no change, 54% decrease, median change of -4 Tg/yr). There is very strong evidence for a drop in biomass burning from TS1 to TS3 (13% increase, 2% no change, 85% decrease, median change of -15 Tg/yr) (Table 7).

5.2 Model Results for the Agricultural Source Scaling with Population

The trends over time in the agricultural and the geologic source strengths are not notably affected by requiring the agricultural source to scale exponentially with world population. The uncertainties about the median source strengths (variances) are reduced and the medians shift slightly (none change by more than 2 Tg/yr) (Figure 2, green boxes). Setting the agricultural source to scale with world population increases the chances of any scenario chosen to explain this data to involve a decrease in the natural$_{Bac}$ source (15% increase, 6% no change, 79% decrease) (Table 7, black-lined boxes). The increase in the agricultural source comes at a time when the global climate system was transitioning from medieval times (which are often considered to have been warm and dry, identified with the Medieval Warm Period in Europe) to the

interval often called the Little Ice Age (which is often considered to have been cooler and wetter). Also, world population growth accelerated during our study interval [McEvedy and Jones, 1978].

5.3 Model Results of the Sensitivity Runs

As expected, isotopic ratios of atmospheric methane are more sensitive to isotopic changes in the larger sources, and are most sensitive to isotopic changes in the sink, as it affects all sources (Table 7). For instance, a +0.001 change in the KIE_{13C} (-1‰ change in the ϵ_{13C} value) of the sink causes the median source strength of biomass burning to shift from 39 Tg/yr during TS1 in the primary run to 24 Tg/yr during TS1 in the sensitivity run (Table 7). However, for the perturbations used here (-1‰ $\delta^{13}C$ and -5‰ δD), the differences between the estimated median source strengths in our sensitivity experiments and the corresponding medians in the primary run were not large, and the general time-trends in median source strengths were not changed (Table 7 and Figure 3).

6 Discussion

6.1 Primary Run Results and Environmental Conditions: 990-1460 CE

The first time slice (TS1) is characterized by relatively low median agricultural emissions, consistent with the relatively low population during this time. In the primary model run, median emissions from biomass burning are higher than estimates in most previous inventories [Ferretti et al., 2005; Lassey et al., 2007] but do agree with values found recently by Fischer et al. [2008] for numerous time intervals from the last glacial maximum to the present. As shown in the sensitivity runs (Table 7), the magnitude of the biomass burning source median can be reduced to agree with Ferretti et al. [2005] by decreasing the ϵ_{13C} of the cumulative methane sink by 1‰, but this adjustment then leaves a higher agricultural source median for the earlier time slices than expected by Ruddiman and Thomson [2001]. The median natural$_{Bac}$ emissions are very close to the pre-industrial estimate used by Lassey et al. [2007], while the median contribution from natural gas venting/leakage is significantly lower than the value presented by Etiope et al. [2008], but much more similar to the value used by Lassey et al. [2007]. The geologic source is nearly constant across all three time slices, with its median never departing by more than 2 Tg/yr from 16 Tg/yr.

6.2 Primary Run Results and Environmental Conditions: 1589-1730 CE

The median agricultural source increased by 60±1% from TS1 to TS3 while the mean increase in world population was ∼38±6%. While 77% of generated scenarios indicate an increase in this source from TS1 to TS3 (Table 7), the entire suite of

scenarios includes those in which a 38% increase in the agricultural source is possible (Figure 2, blue boxes). Still, the median values of this source category at TS1 and TS3 indicate a larger increase in agricultural methane than in population, perhaps reflecting improvements in technology allowing larger areas to be farmed, or a large-scale shift to rice as a major staple due to wetter conditions in the LIA [Hong et al., 2001; Page et al., 2004; Driese et al., 2004; Wang et al., 2005; Paulsen et al., 2003; Chen et al., 2005; Chu et al., 2002; Selvaraj et al., 2007; Anderson et al., 2002; von Rad et al., 1999]. The median biomass burning source strength decreased 38±1% (15 Tg/yr) from TS1 to TS3. Just prior to TS3 there is a sudden ∼20 ppb drop in CH_4 accompanied by a drop in both the δD and $\delta^{13}CH_4$ (Figure 1). A sudden drop in the biomass burning source strength at this time is corroborated by Marlon et al. [2008], and suggested by Ferretti et al. [2005] to be due to the massive plagues that accompanied European contact in the Americas.

Alternatively, Houweling et al. [2008] suggested that the cooling of the LIA indicated by Moberg et al. [2005] was sufficient to explain much of the abrupt 20 ppb drop in CH_4 during the 1580s (also see Etheridge et al. [1998] and Meure et al. [2006]). Decreased temperatures have a negative effect on CH4 emission from wetlands, particulary high latitude wetlands [Worthy et al., 2000]. However, the updated ensemble of Mann et al. [2008] shows the Moberg et al. [2005] record to have a much more pronounced temperature decrease during the MWP/LIA transition than most other records. From Mann et al. [2008] we get a mean temperature change of -0.1 °C and a maximum change of -0.6 °C around the 1580s when the abrupt drop in methane concentrations took place (also see Gerber et al. [2003]). To estimate the impact of this cooling, we follow Houweling et al. [2008]:

$$E_{CH_4} = E^0_{CH_4} * Q_{10}^{\alpha(T^1_{NH} - T^2_{NH})/10}$$

A Q_{10} value of 7 (predicting a 7-fold decrease in methane emission with a 10 °C

decrease in temperature) is selected from the literature [Worthy et al., 2000] and an α value of 1 is retained for simplicity. $E^0_{CH_4}$ is the initial emission rate and E_{CH_4} is the perturbed emission rate taking into account some temperature change defined by T^1_{NH} and T^2_{NH}. According to this relationship, a temperature drop of 0.1 °C would produce only a 2.8 ppb drop in atmospheric methane from a decrease in the global natural$_{Bac}$ emissions alone, while the maximum 0.6 °C drop would result in a 16 ppb decrease. Thus if a uniform temperature decrease and corresponding Q_{10} value is applied to the global natural$_{Bac}$ source, it appears that the maximum Little Ice Age cooling as indicated in the Mann et al. [2008] ensemble approaches the 20 ppb threshold needed to explain the CH_4 decrease in the 1580s CE. However, if the mean temperature change is assumed, additional decreases associated with the biomass burning source (as out model and the work of Marlon et al. [2008] suggest) could explain this CH_4 decrease.

7 Conclusion

New ice-core data from the WAIS Divide site in central West Antarctica document changes in $\delta D(CH_4)$ and $\delta^{13}CH_4$ over the last 1000 years. Our $\delta^{13}CH_4$ data are statistically indistinguishable from those of Ferretti et al. [2005] despite being produced in different laboratories on different ice cores, providing strong confidence that these data successfully record the atmospheric history. Our new $\delta D(CH_4)$ data exhibit time-trends that correlate closely with the $\delta^{13}CH_4$, which is very unlikely to occur if there exist any uncharacterized analytical artifacts, and we conclude that these data also record the atmospheric history. Any hypotheses for the history of atmospheric methane sources and sinks over this important time interval can be tested against the history of atmospheric methane concentration and dual isotopic ratios, as presented here.

Because of the diversity of methane sources, a unique inversion is not possible for the time-history of those sources together with any changes in their isotopic compositions and in methane sinks. We have, however, conducted a simple box-modeling exercise to assess likely histories for the time interval from 990-1730 CE. We chose three time slices within this larger interval when methane concentration and both isotopic ratios were relatively stable. We then attempted to match all three values in all three slices using a simple box model driven by varying strengths of sources assumed to have constant isotopic composition together with constant sink fractionation. We find that an increasing agricultural source and a decreasing biomass-burning source, with most of the change between the 1500s and the 1600s, best fits our data, and that this result is relatively insensitive to the changes in source isotopic compositions or sink isotopic fractionation attempted in this study. The agricultural source scales closely with population, and changes in the biomass burning source may reflect changes in the Americas following European contact, or other processes.

8 Bibliography

References

W. H. Allan, H. Struthers, and D.C. Lowe. Methane carbon isotope effects caused by atomic chlorine in the marine boundary layer: Global results compared with southern hemisphere measurements. *J. Geophys. Res.*, 112:D04306, 2007. doi: 10.1029/2006JD007369.

D. M. Anderson, J. T. Overpeck, and A. K. Gupta. Increase in the asian southwest monsoon during the past four centuries. *Science*, 297:596, 2002. doi: 10.1126/science.1072881.

R. J. Andres, D. J. Fielding, G. Marland, T. A. Boden, N. Kumar, and A. T. Kearney. Carbon dioxide emissions from fossil-fuel use, 1751-1950. *Tellus B*, 51B:759–765, 1999.

M. Battle, M. Bender, T. Sowers, P. P. Tans, J. H. Butler, J. W¿ Elkins, J. T. Ellis, T. Conway, N. Zhang, P. Lang, and A. D. Clark. Atmospheric gas concentrations over the past century measured in air from firn at the South Pole. *Nature*, 383: 231–235, 1996.

P. Bergamaschi. Seasonal variations of stable hydrogen and carbon isotope ratios in methane from a chinese rice paddy. *J. Geophys. Res.-Atmos.*, 102:25383–25393, 1997.

J. P. Chanton, G. J. Whiting, N. E. Balir, C. W. Lindau, and P. K. Bollich. Methane emission from rice: Stable isotopes, diurnal variations, and CO_2 exchange. *Global Biogeochem. Cy.*, 11:15–27, 1997.

J. C. Chen, G. Wan, D. D. Zhang, Z. Chen, J. Xu, T. Xiao, and R. Huang. The

'Little Ice Age' recorded by sediment chemistry in Lake Erhai, southwest China. *The Holocene*, 15, 2005. doi: 10.1191/0959683605hl863rr.

G. Chu, J. Liu, Q. Sun, H. Lu, Z. Gu, W. Wang, and T. Liu. The 'Medieval Warm Period' drought recorded in Lake Huguangyan, tropical South China. *The Holocene*, 12, 2002. doi: 10.1191/0959683602hl566ft.

S. G. Driese, G. M. Ashley, Z. H. Li, V. C. Hover, and R. B. Owen. Possible late Holocene equatorial paleoclimate record based upon soils spanning the Medieval Warm Period and Little Ice Age, Loboi Plain, Kenya. *Paleogeogr. Palaeocl.*, 213: 231–250, 2004.

T. A. Dueck, R. de Visser, H. Poorter, S. Persijn, A. Gorissen, W. de Visser, A. Schapendonk, J. Verhagen, J. Snel, F. J. M. Harren, A. K. Y. Ngai, F. Verstappen, H. Bouwmeester, L. A. C. J. Voesenek, and A. vand der Werf. No evidence for substantial aerobic methane emission by terrestrial plants: a ^{13}C-labelling approach. *New Phytol.*, 2007. doi: 10.1111/j.1469-8137.2007.02103.x.

D. M. Etheridge, L. P. Steele, R. J. Francey, and R. L. Langenfelds. Atmospheric methane between 1000 A.D. and present: Evidence of anthropogenic emissions and climatic variability. *J. Geophys. Res.*, 103:15,979–15,993, 1998.

G. Etiope, Lassey K. R, R. W. Klusman, and E. Boschi. Reappraisal of the fossil methane budget and related emission from geologic sources. *Geophys. Res. Lett.*, 35:L09307, 2008. doi: 10.1029/2008GL033623.

D. F. Ferretti, J. B. Miller, J. W. C. White, D. M. Etheridge, K. R. Lassey, D. C. Lowe, C. M. M. Meure, M. F. Dreier, C. M. Trudinger, and T. D. van Ommen. Unexpected changes to the global methane budget over the past 2000 years. *Science*, 309:1714–1717, 2005.

H. Fischer, M. Behrens, M. Bock, U. Richter, J. Schmidtt, L. Loulergue, J. Chappellaz, R. Spahni, T. Blunier, M. Leuenberger, and T. F. Stocker. Changing boreal methane sources and constant biomass burning during the last termination. *Nature*, 452:864–867, 2008.

S. Gerber, F. Joos, P. Brugger, T. F. Stocker, M. E. Mann, S. Sitch, and M. Scholze. Constraining temperature variations over the last millennium by comparing simulated and observed atmospheric CO_2. *Climate Dynamics*, 20:281–289, 2003.

G. H. Han, H. Yoshikoshi, H. Nagai, T. Yamada, M. Saito, A. Miyata, and Y. Harazonio. Concentration and carbon isotope profiles of CH_4 in paddy rice canopy: Isotopic evidence for changes in CH_4 emission pathways upon drainage. *Chem. Geol.*, 218:25–40, 2005.

Y. T. Hong, Z. G. Wang, H. B. Jiang, Q. H. Lin, B. Hong, Y. X. Zhu, Y. Wang, L. S. Xu, X. T. Leng, and H. D. Li. A 6000-year record of changes in drought and precipitation in northeastern China based on a $\delta^{13}C$ time series from peat cellulose. *Earth Planet. Sci. Lett.*, 185:111–119, 2001.

S. Houweling, F. Dentener, and J. Lelieveld. The modeling of tropospheric methane: How well can point measurements be reproduced by a global model? *J. Geophys. Res.*, 105:8981–9002, 2000.

S. Houweling, F. Dentener, and J. Lelieveld. Simulation of preindustrial methane to constrain the global source strenght of natural wetlands. *J. Geophys. Res.*, 105:17, 243–17,255, 2000b.

S. Houweling, G. R. van der Werf, K. Klein Goldewijk, T. Rockmann, and I. Aben. Early anthropogenic CH_4 emissions and the variation of $\delta^{13}CH_4$

over the last millennium. *Global Biogeochem. Cy.*, 22:GB1002, 2008. doi: 10.1029/2007GB002961.

F. Keppler, J. T. G. Hamilton, M. Brab, and T. Rockmann. Methane emissions from terrestrial plants under aerobic conditions. *Nature*, 439:187–191, 2006.

M. A. K. Khalil, editor. *Stable isotopes in global budgets*. Springer-Verlag., New York., 1993.

M. Knox, P. D. Quay, and D. Wilbur. Kinetic isotopic fractionation during air-water gas ransfer of O_2, N_2, CH_4, and H_2. *J. Geophys. Res.*, 97:20,335–20,343, 1992.

M. Kruger, G. Eller, R. Conrad, and P. Frenzel. Seasonal variation in pathways of CH_4 production and in CH_4 oxidation in rice fields determined by stable carbon isotopes and specific inhibitors. *Glob. Change Biol.*, 8:265–280, 2002.

K. R. Lassey, D. C. Lowe, and M. R. Manning. The trend in atmospheric methane and δ^{13}C and implications for isotopic constraints on the global methane budget. *Global Biogeochem. Cy.*, 14:41–49, 2000.

K. R. Lassey, D. M. Etheridge, D. C. Lowe, A. M. Smith, and D. F. Ferretti. Centennial evolution of the atmospheric methane budget: what do the carbon isotopes tell us? *Atmospheric Chemistry and Physics*, 7:2119–2139, 2007.

I. Levin, P. Bergamaschi, H. Dorr, and D. Trapp. Stable isotopic signature of methane from major sources in Germany. *Chemosphere*, 26:161–177, 1993.

K. Mahieu, A. DeVisscher, P. A. Vanrolleghem, and O. VanCleemput. Carbon and hydrogen isotope fractionation by microbial methane oxidation: Improved determination. *Waste Manage.*, 26:389–398, 2006.

M. E. Mann, Z. Zhang, M. K. Hughes, R. S. Bradley, S. K. Miller, and

S. Rutherford. Proxy-based reconstructions of hemispheric and global surface temperature variations over the past two millennia. *PNAS*, 105:13252–13257, 2008.

T. Marik. Atmospheric δ^{13}C and δD measurements to balance the global methane budget. *PhD Thesis*, Max Plank Institute, 1998.

J. R. Marlon, P. J. Bartlein, C. Carcaillet, D. G. Gavin, S. P. Harrison, P. E. Higuera, F. Joos, M. J. Power, and I. C. Prentice. Climate and human influences on global biomass burning over the past two millennia. *Nature Geoscience*, 1:697–702, 2008.

J. R. McConnell, G. W. Lamorey, S. W. Lambert, and K. C. Taylor. Continuous ice-core chemical analyses using inductively coupled plasma mass spectrometry. *Environ. Sci. Technol.*, 36:7–11, 2002.

C. McEvedy and R. Jones, editors. *Atlas of World Population History*. Penguin Books, Harmondsworth, UK, 1978.

C. MacFarling Meure, D. Etheridge, C. Trudinger, P. Steele, R. Langenfelds, T. van Ommen, A. Smith, and J. Elkins. Law dome CO_2, CH_4 and N_2O ice core records extended to 2000 years BP. *Geophys. Res. Lett.*, 33:L14810, 2006. doi: 10.1029/2006GL026152.

A. Moberg, D. M. Sonechkin, K. Holmgren, N. M. Datsenko, and W. Karlen. Highly variable northern hemisphere temperatures reconstructed from low- and high-resolution proxy data. *Nature*, 433:613–617, 2005.

F. Nakagawa, N. Yoshida, A. Sugimoto, E. Wada, T. Yoshioka, S. Ueda, and P. Vijarnsorn. Stable isotope and radiocarbon compositions of methane emitted from tropical rice paddies and swamps in southern Thailand. *Biogeochemistry*, 61: 1–19, 2002.

R. L. Ott and M. Longnecker, editors. *An Introduction to Statistical Methods and Data Analysis, fifth edition*. Duxbury, Pacific Grove, CA, USA, 2001.

S. E. Page, R. A. J. Wust, D. Weiss, J. O. Rieley, W. Shotyk, and S. H. Limin. A record of late pleistocene and holocene carbon accumulation and climate change from an equatorial peat bog (Kalimantan, Indonesia): implications for past, present, and future carbon dynamics. *J. Quaternary Sci.*, 19:625–635, 2004.

D. E. Paulsen, H. C. Li, and T. L. Ku. Climate variability in central China over the last 1270 years revealed by high-resolution stlagmite records. *Quaternary Sci. Rev.*, 22:691–701, 2003.

J. Pongratz, C. Reick, T. Raddatz, and M. Claussen. A reconstruction of global agricultural areas and land cover for the last millennium. *Global Biogeochem. Cy.*, 22:GB3018, 2008. doi: 10.1029/2007GB003153.

P. Quay, J. Stutsman, D. Wilbur, A. Snover, E. Dlugokencky, and T. Brown. The isotopic compsition of atmospheric methane. *Global Biogeochem. Cy.*, 13:445–461, 1999.

W. S. Reeburgh. Global methane biogeochemistry. *Treatise on Geochemistry*, 4: 65–89, 2004.

A. Rice, A. A. Gotoh, H. O. Aijie, and S. C. Tyler. High-precision continuous-flow measurements of δ^{13}C and δD of atmospheric CH_4. *Anal. Chem.*, 73:4104–4110, 2001.

A. L. Rice, S. C. Tyler, M. C. McCarthy, K. A. Boering, and E. Atlas. Carbon and hydrogen isotopic compositions of stratospheric methane: 1. high-precision observations from the NASA ER-2 aircraft. *J. Geophys. Res.*, 108:D15, 2003. doi: 10.1029/2002JD003042.

W. F. Ruddiman and J. S. Thomson. The case for human causes of increased atmospheric CH_4. *Quaternary Sci. Rev.*, 20:1769–1777, 2001.

F. Rust. Ruminant methane ($\delta^{13}C/\delta D$) values: Relation to atmospheric methane. *Science*, 211:1044–1046, 1981.

G. Saueressig, J. N. Crowley, P. Bergamaschi nad C. Bruhl, C. A. M. Brenninkmeijer, and H. Fischer. Carbon 13 and D kinetic isotope effects in the reactions of CH_4 with O(D) and OH: New laboratory measurements and their implications for the isotopic composition of stratospheric methane. *J. Geophys. Res.*, 106:23,127–23,138, 2001.

K. Selvaraj, C. T. A. Chen, and J. Y. Lou. Holocene east asian monsoon variability: Links to solar and tropical Pacific forcing. *Geophys. Res. Lett.*, 34:L01703, 2007. doi: 10.1029/2006GL028155.

A. L. Sessions, T. W. Burgoyne, and J. M. Hayes. Determination of the H_3 factor in hydrogen isotope ratio monitoring mass spectrometry. *Anal. Chem.*, 73:200–207, 2001.

T. Sowers. Late Quaternary atmospheric CH_4 isotope record suggests marine clathrates are stable. *Science*, 311:838–840, 2006.

T. Sowers, S. Bernard, O. Aballain, J. Chappellaz, J. M. Barnola, and T. Marik. Records of the $\delta^{13}C$ of atmospheric CH_4 over the last 2 centuries as recorded in Antarctic snow and ice. *Global Biogeochem. Cy.*, 19:GB2002, 2005. doi: 10.1029/2004GB002408.

T. A. Sowers, M. L. Bender, and D. Raynaud. Elemental and isotopic composition of occluded O_2 and N_2 in polar ice. *J. Geophys. Res.*, 94:5137–5150, 1989.

C. A. M. Brenninkmeijer T. S. Rhee, M. Brab, and C. Bruhl. Isotopic composition of

H_2 from CH_4 oxidation in the stratosphere and the troposphere. *J. Geophys. Res.*, 111:D23303, 2006. doi: 10.1029/2005JD006760.

P. P. Tans. A note on isotopic ratios and the global atmospheric methane budget. *Global Biogeochem. Cy.*, 11:77–81, 1997.

C. M. Trudinger, I. G. Enting, D. M. Etheridge, R. J. Francey, V. A. Levchenko, and L. P. Steele. Modeling air movement and bubble trapping in firn. *J. Geophys. Res.*, 102:6747–6763, 1997.

M. E. Turner, J. V. Beckett, and B. Afton, editors. *Farm Production in England, 1700-1914*. Oxford University Press, Oxford, UK, 2001.

S. C. Tyler, G. W. Brailsford, K. Yagi, K. Minami, and R. J. Cicerone. Seasonal variations in methane flux and $\delta^{13}CH_4$ values for rice paddies in Japan and their implications. *Global Biogeochem. Cy.*, 8:1–12, 1994.

S. C. Tyler, A. L. Rice, and H. O. Ajie. Stable isotope ratios in atmospheric CH_4: Implications for seasonal sources and sinks. *J. Geophys. Res.*, 112:D03303, 2007. doi: 10.1029/2006JD007231.

M. Uzaki, H. Mizutani, and E. Wada. Carbon isotope composition of CH_4 from rice paddies in Japan. *Biogeochemistry*, 13:159–175, 1991.

U. von Rad, M. Schaaf, K. H. Michels, H. Schulz, W. H. Berger, and F. Sirocko. A 5000-yr record of climate change in varved sediments from the oxygen minimum zone off Pakistan, Northeastern Arabian Sea. *Quaternary Res.*, 51:39–53, 1999.

Y. Wang, H. Cheng, R. L. Edwards, Y. He, X. Kong, Z. An, J. Wu, M. J. Kelly, C. A. Dykoski, and X. Li. The Holocene asian monsoons: Links to solar changes and North Atlantic climate. *Science*, 308, 2005. doi: 10.1126/science.1106296.

D. E. J. Worthy, I. Levin, F. Hopper, M. K. Ernst, and N. B. A. Trivett. Evidence for a link between climate and northern wetland methane emissions. *J. Geophys. Res.*, 105:4031–4038, 2000.

D. J. Wuebbles and K. Hayhoe. Atmospheric methane and global change. *Earth-Sci. Rev.*, 57:177–210, 2002.

K. Yamada, Y. Ozaki, F. Nakagawa, S. Sudo, and H. Tsuruta. Hydrogen and carbon isotopic measurements of methane from agricultural combustion: Implications for isotopic signatures of global biomass burning sources. *J. Geophys. Res.*, 111: D16306, 2006. doi: 10.1029/2005JD006750.

Table 1: Verification of Analytical Method

System Tested	**Method**	**N**	δ^{13}**C(‰)**	**std dev**	**Meas. - Accept.[a]**
Analytical	Flask[b]	100	-46.9	0.1	0.2
Extraction	BFI[c]	16	-47.4	0.2	-0.3
System Tested	**Method**	**N**	δ**D(‰)**	**std dev**	**Meas. - Accept.[a]**
Analytical	Flask[b]	46	-86	3	-2
Extraction	BFI[c]	5	-85	2	-1

[a]Accepted value provided by Stan Tyler (UCI), CH_4 Std.(Tyler)= 1776ppb, δ^{13}C = -47.16 ‰, δD = -84.3 ‰ [b]Std equilibrated into glass flasks and put directly into the analytical system [c]Std equilibrated over bubble free ice (BFI) and ran through both the extraction system and the analytical system

A Verification of Analytical Method

Table 2: Corrected Data Set for all δD data

Extraction Date	Sample Mass (g)	Mean Sample Depth (m)	Ice Age (yr. CE)	Sample δ^{13}C (‰)
9/12/2007	1572	69.88	1771.37	-94.35
9/20/2007	1400	73.75	1755.80	-91.36
9/11/2007	1488	81.758	1721.81	-119.10
9/15/2007	1560	85.91	1704.86	-95.15
9/13/2007	1593	89.175	1691.52	-91.80
9/24/2007	1567	93.81	1672.20	-94.60
9/13/2007	1572	97.62	1657.79	-95.16
9/12/2007	1553	105.42	1626.72	-98.25
9/7/2007	1630	114.575	1587.28	-100.88
9/11/2007	1596	118.13	1571.41	-87.38
9/18/2007	1637	122.38	1553.88	-90.24
9/10/2007	1589	125.68	1539.90	-93.92
9/18/2007	1653	130.06	1521.64	-87.33
9/6/2007	1580	133.725	1506.38	-90.07
9/21/2007	1590	137.55	1490.63	-90.56
9/17/2007	1700	141.525	1471.98	-87.52
9/4/2007	1473	146.565	1451.64	-92.61
9/17/2007	1560	150.41	1434.30	-83.42
9/20/2007	1627	153.365	1421.24	-80.70
9/19/2007	1610	157.52	1403.09	-87.23
9/19/2007	1583	161.185	1387.35	-80.71
9/27/2007	1430	164.68	1372.23	-87.83
9/4/2007	1645	169.105	1350.83	-88.45
9/21/2007	1563	173.15	1333.81	-89.64
9/28/2007	1657	175.47	1322.54	-83.34
9/26/2007	1712	176.995	1315.69	-87.55
9/25/2007	1612	181.45	1293.21	-86.06
9/26/2007	1623	185.72	1271.48	-82.37
8/24/2007	1600	189	1256.25	-75.97
8/21/2007	1500	193.665	1234.63	-75.11
8/30/2007	1288	197.03	1220.06	-84.11
8/21/2007	1540	197.32	1218.68	-81.24
8/16/2007	1500	201.47	1199.41	-80.02
8/29/2007	1600	203.19	1190.23	-84.15
8/30/2007	1509	204.13	1185.68	-82.32
8/24/2007	1460	205.17	1181.00	-80.81
9/10/2007	1593	221.75	1102.85	-84.34
9/28/2007	1595	237.93	1031.69	-79.82
9/7/2007	1485	245.47	996.07	-81.34
9/24/2007	1640	249.62	978.20	-87.56
9/6/2007	1673	253.56	960.58	-85.71

This table contains all δD(CH_4) generated in this study. This data was used to constrain the model results.

B Corrected Data Set for all δD data

C Corrected Data for δ^{13}C (2007)

Table 3: Corrected Data for δ^{13}C (2007)

Extraction Date	Sample Mass (g)	Mean Sample Depth (m)	Ice Age (yr. CE)	Sample δ^{13}C (‰)
10/23/2007	455	70.14	1770.40	-47.55
9/13/2007	787	81.455	1722.77	-48.02
10/2/2007	825	89.4	1690.63	-48.46
10/23/2007	485	93.02	1675.50	-49.74
10/2/2007	805	97.9	1656.75	-48.51
9/10/2007	865	114.22	1589.28	-48.17
10/1/2007	860	125.9	1539.14	-47.30
9/18/2007	817	130.33	1520.47	-48.75
10/1/2007	790	137.79	1489.18	-47.95
10/22/2007	455	141.73	1471.13	-48.49
11/6/2007	440	141.845	1470.60	-48.48
10/18/2007	845	146.82	1450.57	-48.44
9/16/2007	886	150.65	1433.11	-48.39
10/1/2007	820	153.101	1422.39	-48.16
10/19/2007	755	157.8	1401.91	-48.46
9/11/2007	865	169.375	1349.97	-47.06
11/2/2007	410	177.185	1314.91	-47.53
9/6/2007	847	188.705	1257.68	-47.02
8/29/2007	593	193.9	1233.67	-47.76
8/2/2007	630	194.39	1231.71	-48.36
8/6/2007	485	194.49	1231.12	-47.78
9/6/2007	837	194.525	1230.94	-47.05
8/7/2007	485	196.075	1224.66	-46.84
10/18/2007	590	211.57	1150.77	-47.58
10/30/2007	373	215	1134.63	-48.54
10/30/2007	472	215.08	1134.33	-47.49
8/30/2007	636	215.75	1131.14	-47.89
10/18/2007	707	216.64	1126.89	-47.48
11/8/2007	370	238.02	1031.13	-48.21
11/9/2007	350	238.08	1030.79	-46.19
11/7/2007	375	249.82	977.35	-48.16
9/5/2007	855	253.835	958.88	-47.37
11/5/2007	425	257.54	942.20	-47.60
11/9/2007	340	261.94	922.30	-47.64
11/5/2007	390	262.16	921.38	-48.13
11/8/2007	383	266	905.19	-48.14
11/7/2007	333	266.11	904.65	-45.99
11/9/2007	370	276.5	856.48	-46.37
11/6/2007	455	276.625	855.86	-46.70
9/6/2007	837	281.055	834.37	-47.13
8/1/2007	745	283.835	821.75	-46.80
11/7/2007	338	283.985	821.07	-46.88
11/5/2007	398	292.28	775.70	-46.48
11/2/2007	393	296.195	756.18	-47.43

This table contains all $\delta^{13}CH_4$ generated during 2007. This data was not used to constrain the model results. During the generation of this data, the verification process using bubble-free ice had yet to be perfected. As a result the verification runs were tainted by copper flecks from the gasket used to seal the sample cylinder. This problem was addressed by using gold-plated gaskets to generate the bubble-free ice. Also, mid-way through the generation of these data the melting bath switched from being warmed by hot water continually flowing from the tap, around the cylinder, and down the drain, to warming a single pot of water (with the sample cylinder in it) with a hot plate. The temperature of this hotplate was not strictly controlled and no verification runs were used to make certain that it did not corrupt the true atmospheric value of the sample. During some runs this water bath become too hot causing the copper gasket to degrade and thereby introducing copper flecks into the sample, thus changing the resulting isotopic composition of the sample. Once this was found out the temperature of the hotplate was regulated much more strictly. Also, during 2007 there were two operators of the extraction system. It is possible that this could have also affected our results. In 2008 only one operator generated all the data. Thus, this data was not used to constrain our model output, but all problems encountered to generate this data set were fixed in order to produce the high-quality data set of $\delta^{13}CH_4$ generated during 2008.

D Corrected Data for δ^{13}C (2008)

Table 4: Corrected Data for δ^{13}C (2008)

Extraction Date	Sample Mass (g)	Mean Sample Depth (m)	Ice Age (yr. CE)	Sample δ^{13}C (‰)
4/18/2008	525	70.24	1770.00	-48.83
5/15/2008	455	73.95	1754.76	-48.80
5/26/2008	423	74.07	1754.06	-48.60
5/27/2008	495	77.495	1739.06	-48.30
5/16/2008	517	77.61	1738.52	-48.82
5/30/2008	690	83.03	1716.78	-48.37
5/30/2008	499	85.59	1706.21	-48.84
5/15/2008	528	85.7	1705.78	-48.95
6/2/2008	690	93.24	1674.80	-48.75
4/22/2008	497	94.14	1670.90	-49.61
5/20/2008	617	101.245	1644.15	-48.62
5/14/2008	542	105.63	1625.68	-48.50
5/19/2008	543	111.44	1600.77	-48.86
5/26/2008	496	117.74	1573.38	-49.03
4/23/2008	550	117.87	1572.72	-49.26
4/13/2008	715	122.62	1552.68	-49.08
5/20/2008	565	125.255	1541.73	-48.68
5/27/2008	710	125.45	1540.91	-48.13
4/23/2008	532	133.935	1505.67	-49.24
5/17/2008	545	138.07	1487.67	-49.30
5/17/2008	540	138.18	1487.26	-49.18
5/21/2008	577	161.45	1386.23	-47.91
5/26/2008	490	162.635	1380.93	-48.39
5/19/2008	579	164.96	1370.62	-48.25
6/3/2008	510	169.8	1348.24	-47.84
5/14/2008	561	173.36	1332.67	-47.76
4/18/2008	598	175.68	1321.73	-47.82
4/10/2008	623	177.305	1314.48	-47.84
5/30/2008	591	181.66	1291.96	-47.67
5/29/2008	590	185.38	1273.00	-47.90
4/24/2008	595	185.51	1272.41	-47.91
5/27/2008	530	189.865	1252.50	-47.03
5/23/2008	490	193.33	1236.67	-47.28
5/14/2008	510	193.46	1235.92	-47.13
6/2/2008	620	198.53	1213.27	-47.51
4/25/2008	435	199.92	1206.35	-50.13
4/28/2008	525	201.13	1200.95	-47.78
4/28/2008	533	201.26	1200.26	-47.20
5/29/2008	490	205.91	1177.23	-47.31
5/21/2008	603	208.98	1163.32	-47.33
4/10/2008	740	211.38	1151.81	-47.33
4/3/2008	600	213	1144.41	-47.94
4/3/2008	680	213.47	1142.29	-47.45
5/17/2008	570	213.585	1141.71	-47.68
5/16/2008	578	216.905	1125.92	-47.30
4/23/2008	665	221.52	1103.90	-47.62
5/22/2008	612	225.245	1087.10	-47.60
5/15/2008	529	229.29	1068.84	-47.79
5/28/2008	605	229.73	1067.03	-47.04
5/17/2008	593	233.05	1052.14	-47.25
5/28/2008	465	239.095	1025.78	-47.25
5/16/2008	567	242.045	1012.50	-47.48
4/3/2008	360	245.65	995.36	-43.63
4/18/2008	555	245.78	994.80	-47.38
5/22/2008	675	249.17	980.13	-47.19
4/17/2008	495	249.95	976.88	-48.71
5/22/2008	455	256.76	946.15	-47.52
5/21/2008	563	261.255	924.98	-47.58
5/20/2008	547	278.77	845.41	-47.06
5/19/2008	505	289.345	791.52	-47.32

This table contains all $\delta^{13}CH_4$ generated during 2008. This data was used to constrain the model results.

Table 5: Source Parameters used For Model Runs

Source	Emission Range Tg/yr (10^{12} g/yr)		Step Tg/yr	$\delta^{13}C$[a] ‰	δD[a] ‰	NH[b] %	SH[b] %
Agricultural	60[i]	0	1	-63±5[j]	-330±15[j]	80	20
Geologic	53[e]	5[f]	1	-38±7[k]	-175±20[k]	90	10
$Natural_{Bac}$	232[c]	92[c]	1	-57[d]±5[k]	-322±20[k]	77	23
Biomass Burning	45[g]	5[f]	1	-23.6±2[h]	-169±21[h]	44	56

[a]Mean isotope values were used in the model, ranges are shown only to indicate the uncertainty in each value[b]Hemispheric distribution of sources taken from Marik [1998][c]Emission Range taken that of wetlands from Wuebbles and Hayhoe [2002], and references therein.[d]Weighted average of all natural bacterial sources (termites, tundra, lakes, swamps and marshes) with relative contributions and isotope values taken from the budget of Tyler et al. [2007], and references therein.
[e]Maximum value taken as the mean from Etiope et al. [2008][f]Taken from mean value for preindustrial emissions in Lassey et al. [2007][g]Mean value suggested from model runs by Fischer et al. [2008] [h]Mean global value and uncertainties calculated from Yamada et al. [2006][i]Based on the maximum value suggested by Ruddiman and Thomson [2001] at 1700 CE[j]The mean isotopic values for the agricultural source were determined by weighting the isotopic values of rice cultivation and animal husbandry by the emission values from Lassey et al. [2007]. The isotopic value for rice was determined using the studies of [Uzaki et al., 1991; Levin et al., 1993; Tyler et al., 1994; Bergamaschi, 1997; Chanton et al., 1997; Kruger et al., 2002; Nakagawa et al., 2002; Han et al., 2005]and the isotopic value for CH_4 released from the rumen of farm animals was determined using the studies of Rust [1981] and Levin et al. [1993][k]Uncertainties taken from Quay et al. [1999]

E Source Parameters used For Model Runs

Table 6: Sink Kinetic Isotope Effect (KIE) values used in model runs

Sink	Relative Contribution[e] (%)	KIE $k(^{13}CH_4)/k(^{12}CH_4)$	KIE $k(^{12}CH_3D)/k(^{12}CH_4)$
Troposphere	88±2.9	0.9961±0.0004[a]	0.7729±0.0108[a]
Stratosphere	7±2.6	0.9847±0.0047[b]	0.7005±0.0294[c]
Soils	5±3.4	0.9824±0.0032[d]	0.8764±0.0795[d]
Total[f]	—	**0.9946±0.0008**	**0.7731±0.0155**

[a]Saueressig et al. [2001] [b]Mean value for range in Rice et al. [2003] [c]T. S. Rhee et al. [2006] [d]Average of mean values found in Mahieu et al. [2006], and references therein [e]Relative contributions from each sink determined by the sink strengths found in Reeburgh [2004], and references therein [f]The total CH_4 sink magnitude was parameterized via the lifetime of CH_4 (held constant at 7.6 years for all model runs)

F Sink Kinetic Isotope Effect (KIE) values used in model runs

Table 7: Median Source Strengths for many Run Types

Type of Run	Value Shifted	Category Shifted	Result Source Category	Medians TS1[a]	Medians TS3[a]	Median Diff.[b]	% of Scenarios +[c]	% of Scenarios =[d]	% of Scenarios −[e]
Primary Run	*NA*	*NA*		*12*	*30*	*18*	*77*	*2*	*21*
Ag. scale w/pop.	NA	NA		11	30	19	NA	NA	NA
Sensitivity	$\delta^{13}C$	Biomass Burning		10	29	19	81	2	17
Sensitivity	δD	Biomass Burning		13	31	18	76	2	22
Sensitivity	$\delta^{13}C$	Geologic		11	29	18	79	2	19
Sensitivity	δD	Geologic		13	31	18	78	2	21
Sensitivity	$\delta^{13}C$	Agricultural	Agriculture	10	28	18	81	2	18
Sensitivity	δD	Agricultural		14	31	17	76	2	22
Sensitivity	$\delta^{13}C$	Natural_{Bac}		2	20	18	91	3	7
Sensitivity	δD	Natural_{Bac}		20	39	19	76	1	22
Sensitivity	$\delta^{13}C$	Sink		30	46	16	73	2	26
Sensitivity	δD	Sink		4	19	15	85	3	12
Primary Run	*NA*	*NA*		*16*	*18*	*2*	*59*	*5*	*37*
Ag. scale w/pop.	NA	NA		16	19	3	63	4	33
Sensitivity	$\delta^{13}C$	Biomass Burning		15	18	3	60	5	36
Sensitivity	δD	Biomass Burning		17	19	2	56	5	39
Sensitivity	$\delta^{13}C$	Geologic		15	18	3	60	5	36
Sensitivity	δD	Geologic		17	19	2	59	4	37
Sensitivity	$\delta^{13}C$	Agricultural	Geologic	16	18	2	56	5	39
Sensitivity	δD	Agricultural		16	20	4	63	4	33
Sensitivity	$\delta^{13}C$	Natural_{Bac}		14	14	0	48	7	45
Sensitivity	δD	Natural_{Bac}		24	26	2	52	4	43
Sensitivity	$\delta^{13}C$	Sink		24	23	-1	42	5	53
Sensitivity	δD	Sink		4	10	6	67	9	24
Primary Run	*NA*	*NA*		*185*	*181*	*-4*	*44*	*1*	*54*
Ag. scale w/pop.	NA	NA		187	181	-6	15	6	79
Sensitivity	$\delta^{13}C$	Biomass Burning		187	182	-5	41	1	57
Sensitivity	δD	Biomass Burning		184	180	-4	46	1	52
Sensitivity	$\delta^{13}C$	Geologic		186	182	-4	45	1	54
Sensitivity	δD	Geologic		184	179	-5	45	1	54
Sensitivity	$\delta^{13}C$	Agricultural	$\text{Natural}_{\text{Bac}}$	188	183	-5	45	1	54
Sensitivity	δD	Agricultural		183	179	-4	46	1	53
Sensitivity	$\delta^{13}C$	Natural_{Bac}		190	185	-5	39	2	59
Sensitivity	δD	Natural_{Bac}		175	170	-5	44	1	55
Sensitivity	$\delta^{13}C$	Sink		174	170	-4	47	1	51
Sensitivity	δD	Sink		197	195	-2	48	2	51
Primary Run	*NA*	*NA*		*39*	*24*	*-15*	*13*	*2*	*85*
Ag. scale w/pop.	NA	NA		38	24	-14	10	2	88
Sensitivity	$\delta^{13}C$	Biomass Burning		39	25	-14	12	2	86
Sensitivity	δD	Biomass Burning		38	24	-14	13	2	85
Sensitivity	$\delta^{13}C$	Geologic		40	25	-15	11	2	87
Sensitivity	δD	Geologic		38	23	-15	13	2	85
Sensitivity	$\delta^{13}C$	Agricultural	Biomass	39	26	-13	16	2	82
Sensitivity	δD	Agricultural	Burning	39	23	-16	11	2	87
Sensitivity	$\delta^{13}C$	Natural_{Bac}		44	35	-9	5	4	91
Sensitivity	δD	Natural_{Bac}		32	18	-14	18	2	80
Sensitivity	$\delta^{13}C$	Sink		24	13	-11	21	3	76
Sensitivity	δD	Sink		43	28	-15	3	1	96

[a]TS1 and TS3 denote time slice one (990-1460 CE) and time slice three (1589-1730 CE). They were chosen to analyze the maximum variability in the data set. [b]This is calculated as TS3−TS1.[c]Denotes the percent of all scenarios in the indicated run type for which the source strength of the indicated source category was greater during TS3 than at TS1.[d]Denotes the percent of all scenarios in the indicated run type for which the source strength of the indicated source category was constant for both TS3 and TS1.[e]Denotes the percent of all scenarios in the indicated run type for which the source strength of the indicated source category was less during TS3 than at TS1.

G Median Source Strengths for many Run Types

H δ^{13}C, δD, and CH_4 data

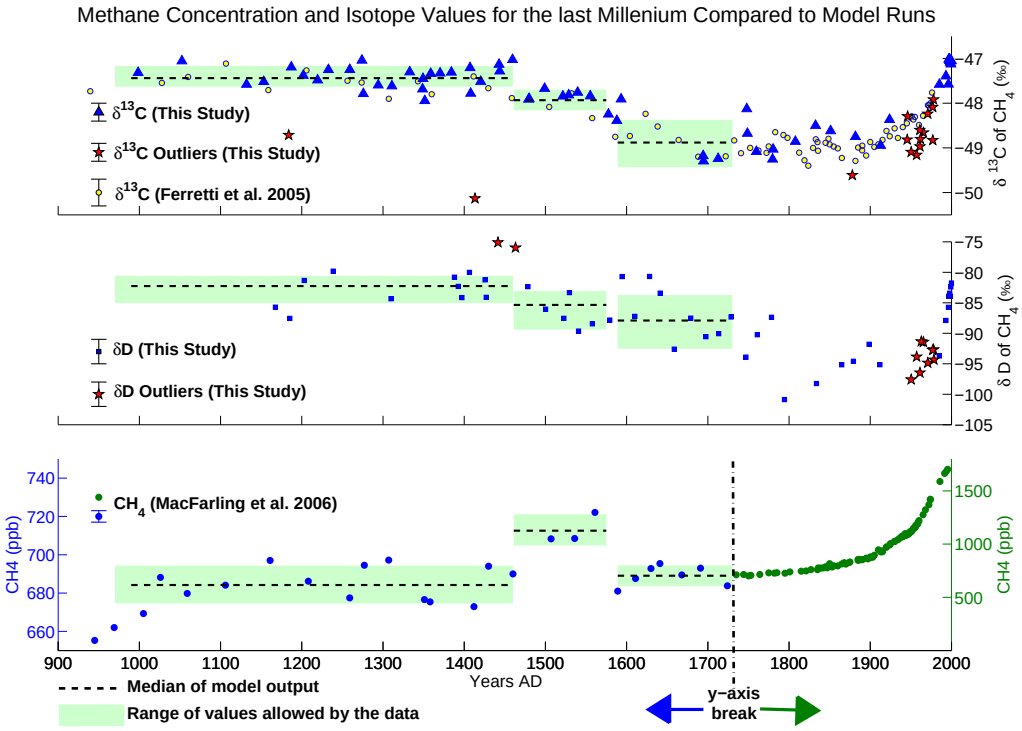

Figure 1: δ^{13}C, δD, and CH_4 data

The time scales for the isotopic data are shifted backwards 20 years relative to the time scale for the CH_4 concentration data in order to account for the lag in the equilibrium of the isotopes relative to the concentration as discussed in Tans [1997]. The $\delta^{13}CH_4$ and $\delta D(CH_4)$ data from 1950 CE to the present are from analysis of the firn air from the WAIS Divide WDC05A site. The shaded regions are defined as the range of values per data set per time slice that a model run must match in order to be considered a valid scenario for that time slice. These ranges are defined as one standard deviation from the average for each constraint for each time slice. The black dashed horizontal lines included in the shaded regions denotes the median values for each constraint as modeled in the primary run. Note that the y-axis for the CH_4 concentration plot is split at 1730 (denoted by a vertical dashed line), with all points later than 1730 being plotted on the right y-axis and all points earlier than 1730 being plotted on the left y-axis.

I Box plot of Model Results

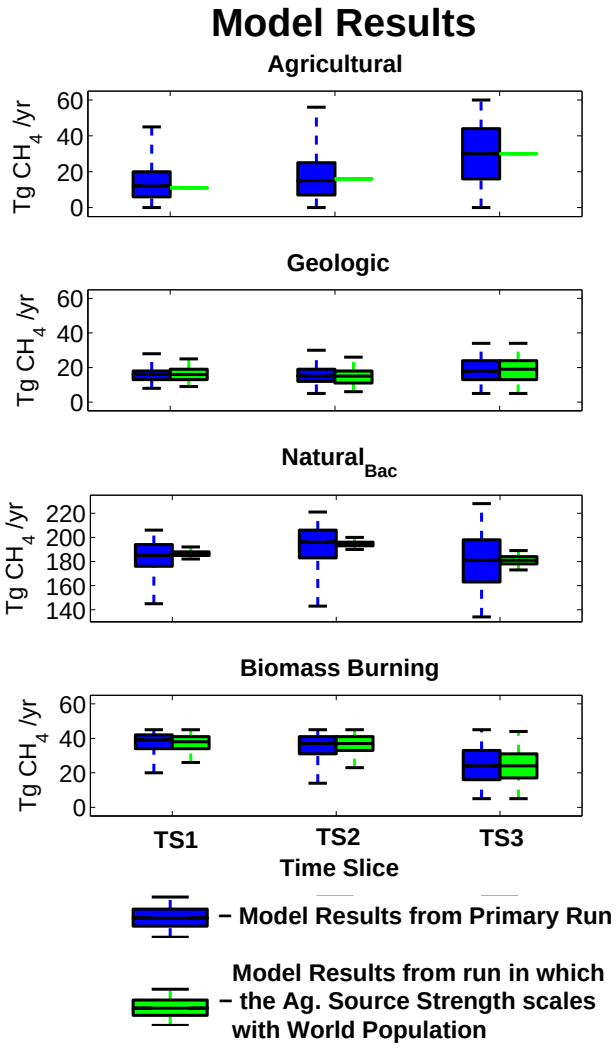

Figure 2: Box plot of Model Results

This box plot contains two model run types. The first (blue boxes) displays data from the primary run and the second (green boxes) displays data from the "agriculture scaling with population" run type or AgP. The data for the AgP run displayed in the agricultural source plot are singular values (the median values for the primary run) and were prescribed in the AgP model run type. Notice that trends in the AgP run are similar to those in the primary run, just with less variance about the means.

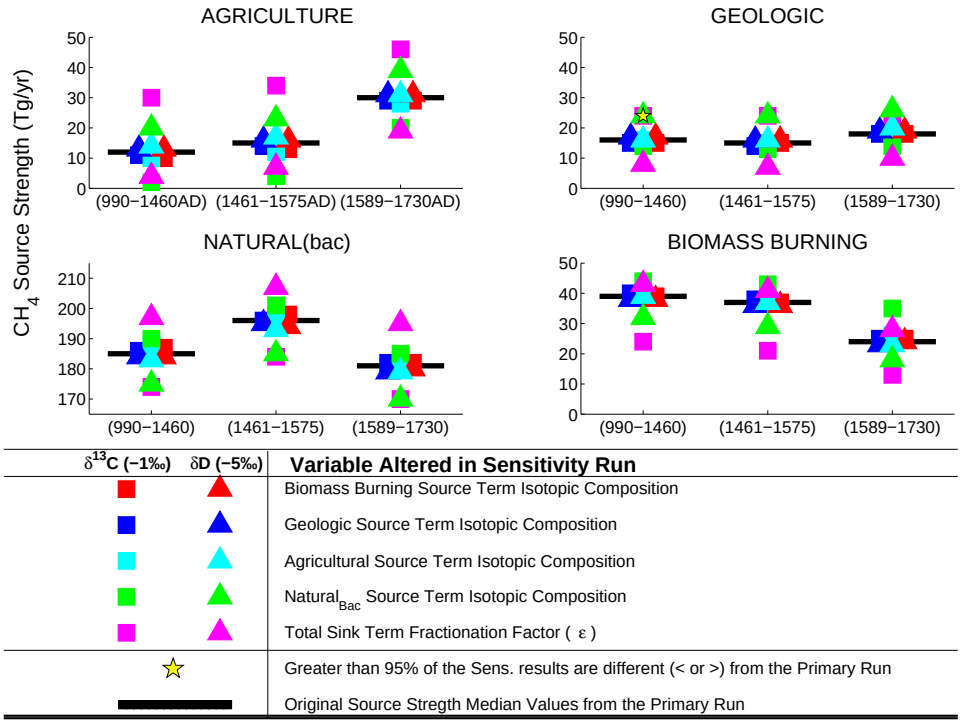

Figure 3: Sensitivity Results

This is a plot displaying all the medians generated by all the sensitivity runs. The medians from the primary runs are displayed as horizontal black bars for reference.

J Sensitivity Studies